Geosynthetics - 7th ICG - Delmas, Gourc & Girard (eds) © 2002 Swets & Zeitlinger, Lisse ISBN 90 5809 523 1

Fem analysis of reinforced segmental retaining walls with cohesive and granular backfills

E. GULER & M. HAMDERI, Bosphorus University, Istanbul, Turkey

ABSTRACT: The actual failure mechanisms of the reinforced earth segmental walls with extensible reinforcements are studied with a FEM package program. The failure mechanism suggested by the program was compared with current design methods. For both cohesive and granular backfills, the developing failure surface is gradually shifted to a direct sliding mode as failure approached.

1 INTRODUCTION

The design of segmental retaining structures is commonly performed by using Limit Equilibrium Analysis. However for the analysis to reflect the reality, the failure planes have to be determined properly. The failure planes used in the design codes reflect the findings of failure planes determined for classical retaining structures and were adapted to metal reinforcement. This adaptation gradually included the geosynthetic reinforcement. To investigate the validity of these assumptions a F.E.M. analysis was performed and comments were made on the results comparing to manual design considerations.

2 PREVIOUS RESEARCH

Several different techniques were proposed to investigate the actual failure mechanisms of the reinforced earth walls with finite element analysis. In these techniques, the investigated system's parameters are increased or reduced to a certain level to establish a failure. One of the techniques is the shear reduction technique proposed by Matsui and San (1988) to the finite element stability analysis. In this technique, the shear strength parameters, cohesion, c, and coefficient of friction, tan ϕ, where ϕ is the angle of internal friction, of the component materials are incrementally reduced by dividing them with a common shear strength reduction ration R. The failure mechanism of a cut slope is examined (Matsui and San 1988) by using shear strain failure criterion (strain-based failure judgment method). The shear failure of an element is defined as the shear strain level exceeding the failure shear strain. Another technique proposes gradually reducing the K_0 in subsequent runs from its empirical value (K_0 = 1- sin ϕ) until the failure of the slope occurred using the strain based failure judgment method (San, Leshchinsky and Matsui 1994).

3 FEM DETAILS

3.1 *F.E. Program*

Finite Element Analysis is performed by Plaxis BV finite element package program. Failure surface evaluations are considered at the end of two main phases. The first phase represents the construction process and the second phase is the phi-c reduction. Phi-c reduction is the same shear strength reduction technique that was mentioned above. The shear strength parameters, coefficient of friction tan ϕ, and the cohesion c are incrementally reduced by dividing them with a reduction factor *ΣMsf* at a given stage in the analysis:

$$\Sigma Msf = \frac{tan\phi_{input}}{tan\,\phi_{reduced}} = \frac{c_{input}}{c_{reduced}} \quad (1)$$

where ϕ_{input} = initial friction angle of the soil, $\phi_{reduced}$ =friction angle of the soil after reduction, c_{input} = initial cohesion of the soil, $c_{reduced}$ = cohesion of the soil after reduction. The program reduces these parameters in small increments by increasing the value of ΣMsf. After each successive reduction of the ΣMsf value, the system is checked for equilibrium. Where equilibrium can not be sustained any more, the value of ΣMsf at this point can be defined as the factor of safety of the model (Figure 7). Also, incremental shear strain zones are considered as the potential failure patterns.

3.2 *Model*

In the 2D analyses two-dimensional and 6-node triangle elements are selected. It provides a second order interpolation for displacements. The element stiffness matrix is evaluated by numerical integration using a total of three Gauss points (stress points) illustrated in Figure 1.

In all the models the wall height is chosen 9 m, the width of the backfilled zone is 25 m, the foundation soil depth is 5 m. Investigated parameters are soil type, reinforcement length and reinforcement vertical spacing. There are three reinforcement lengths (L) 4.5, 6 and 9 m. 0.5 m and 1 m reinforcement vertical spacing (S_v) are used. These combinations are repeated for frictional and cohesive backfill. Altogether, 12 models are taken into consideration (Table 1). Typical representative model B3 is shown in Figure 2.

Table 1. Model combinations

A	L/H	ϕ	c	S_v	*B*	L/H	ϕ	c	S_v
1	0.5	35	5	0.5	*1*	0.5	35	5	1
2	0.5	5	50	0.5	*2*	0.5	5	50	1
3	0.67	35	5	0.5	*3*	0.67	35	5	1
4	0.67	5	50	0.5	*4*	0.67	5	50	1
5	1	35	5	0.5	*5*	1	35	5	1
6	1	5	50	0.5	*6*	1	5	50	1

Wall facings elements are constituted with segmental block elements. The segmental blocks are modeled in the 2D model with elements of 50 cm width and 25 cm height. Block elements were separated with interface elements. The strength properties of interfaces are linked to the strength properties of the soil layer.

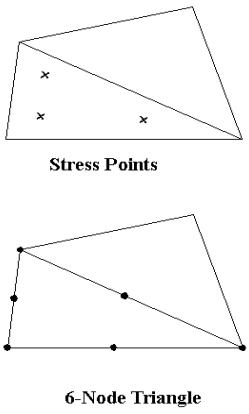

Figure 1. Mesh element

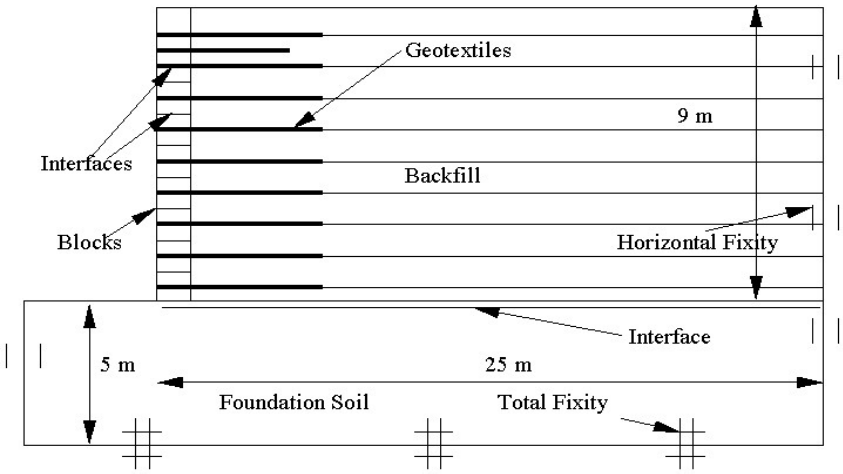

Figure 2. Representative model B3

Each soil data has an associated strength reduction factor for interfaces (R_{inter}). The interface properties are calculated from the soil properties in the associated data set and the strength reduction factor by applying the following rules:

$$c_i = R_{inter}\, c_{soil} \quad (2)$$

$$\tan\phi_i = R_{inter}\, \tan\phi_{soil} \leq \tan\phi_{soil} \quad (3)$$

where c_i = cohesion at interface; ϕ_i = friction angle at interface; R_{inter} = strength reduction factor; c_{soil} = soil cohesion; ϕ_{soil} = soil internal friction angle. R_{inter}=0.85 value is taken for the block elements and for soil types. The geotextiles are laid horizontally and their ends on the wall side are fixed between two blocks with an interface.

3.3 *Material Properties*

The backfill soil is modeled as a homogeneous elasto-plastic Mohr Coulomb material. Two types of soil are used for backfilling. The first type is a granular soil having an internal friction angle of 35° and cohesion of 5 kN/m^2. The second type is a cohesive soil having cohesion of 50 kN/m^2 and an internal friction angle of 5°.

The same elasto-plastic Mohr Coulomb material model is also used for both the segmental blocks and the foundation soil. In order not to allow for any failure inside the foundation soil, high cohesion (c=200 kN/m^2) and internal friction angle (ϕ=35°) values are assigned for the foundation soil. Similarly, high cohesion value of 200 kN/m^2 and an internal friction angle of 35° are assigned to the segmental blocks. The segmental elements are given a higher Young's modulus of 300 000 kN/m^2. This value is 30 000 kN/m^2 in backfill soil and 50 000 kN/m^2 in foundation soil. No dilatancy is attributed to any soil. Every soil type has the density of 20 kN/m^3.

Geotextiles are defined as tensional-elastic elements. All the geotextiles have the same Elastic modulus of 1 500 kN/m. These elements have infinitive strain property and no cut value in a certain tension. However, the tensile forces of the geotextiles were checked and normally do not exceed the typical strength values. No ground water table is considered. .

3.4 *Analysis*

In order to simulate the real case, three main phases can be defined. The first phase is the initial phase, which is implemented to generate initial stresses according to the coefficient of lateral earth pressure K_o. In the initial phase, only foundation soil is taken into consideration to generate initial stresses and deformations. In the second phase, staged construction was applied in lifts 0.5 m and 1 m respectively. The self-weight of each lift was applied incrementally. After stage construction, phi-c reduction was implemented as the third phase.

All the data during construction phases such as displacements, stresses and strain is brought together to generate animation.

4 RESULTS

Shear strains, incremental shear strains, deformed mesh and maximum tensile stresses were used for evaluation. For granular soils B3 model was chosen as representative. The shear strains output at the end of the *staged construction* in *B3 system* is illustrated in Figure 3.

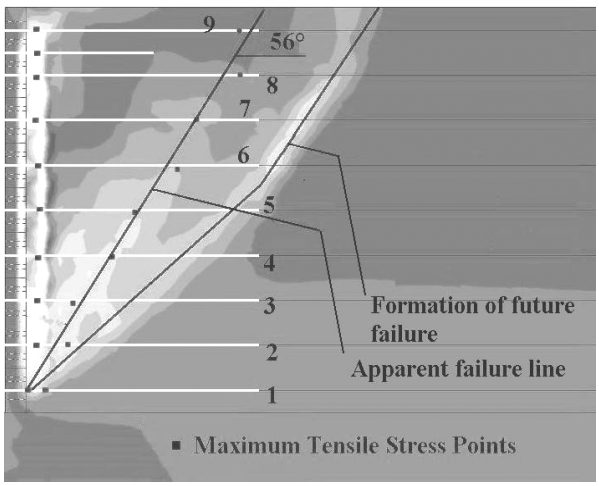

Figure 3. Shear Strain Shadings at the end of the staged construction in B3

There are three different zones where the shear strains are concentrated. The first zone seems to appear just at the back of the blocks. Strain concentration reduces behind the blocks at the top and the bottom.

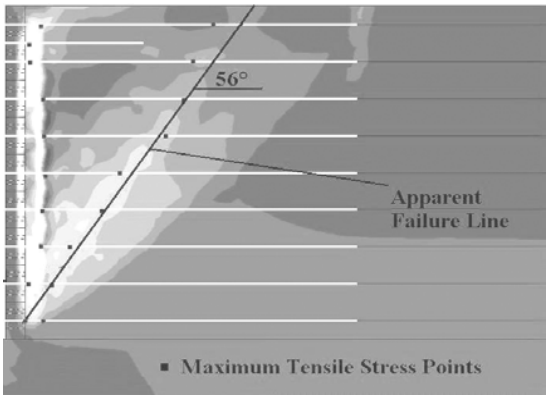

Figure 4. Shear strain shadings at the end of the staged construction in B5

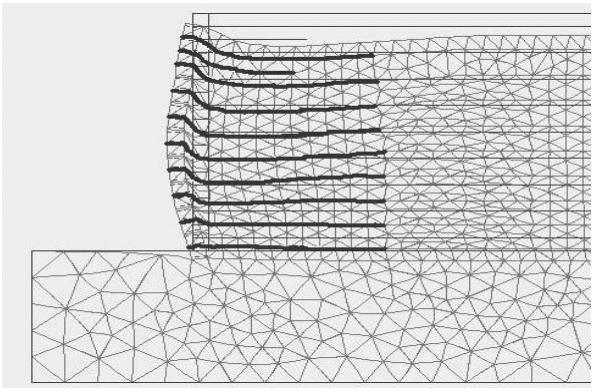

Figure 5. Deformed mesh at the end of the staged construction B3 (displacements scaled up 20 times)

Table 2. Tensile forces in B3 model

Reinf. No	Distance from left (m)	Force* (kN)	Distance from left (m)	Force** (kN)
9	1	4.0	5.5	2.8
8	1	5.9	5.5	2.8
7	1	10.5	4.5	5.9
6	1	12.1	4	7.63
5	1	12.7	2.5	9
4	1	13.2	2.5	10.2
3	1	13.4	1.5	10.7
2	1	8.9	1.5	7.9
1	0.5	3.5	1	7

* Peak tensile force right behind the blocks

** Peak tensile force in the remaining length

The second shear strain concentration zone, which is believed to be the apparent failure surface, seems to appear as a linear line represented in Figure 3. The line makes approximately an angle of 56° with the horizontal. The failure surface mechanism for the walls with extensible reinforcement is assumed to occur with an angle of $45+\phi/2$ (62.5° for our systems) starting from the toe of the wall. According to this, apparent failure line obtained from the shear strain output data and the assumed failure surface appear to be reasonably close. There is a third bilinear shear strain concentration zone forming just below the apparent failure line. This additional shear concentration is supposed to dominate in the formation of the actual failure line in the phi-c reduction process. In model B5, since the reinforcement lengths are longer this additional concentration has not developed at the end of the staged construction (Figure 4). The maximum horizontal displacement is obtained in the mid-height of the wall and has a value of 3.2 cm. As the deformed mesh is studied (Figure 5), it is noticeable that top and the bottom blocks make less horizontal deformation compared to the ones in the middle, because, less horizontal stress causes less deformation at the top and the base friction resists the bottom blocks to move horizontally despite the high horizontal stresses at the bottom. Besides, when the tensile forces on the top and bottom reinforcements are studied, it is noticeable that they have comparatively smaller force than the centrally located reinforcements (Table 2).

Tensile forces on the reinforcements at the end of the staged construction are in the range of 5 kN/m and 15 kN/m (Table 2). Breakage of reinforcements is not expected because; those tensile forces are bearable for almost all reinforcement types. Maximum tensile stress locations on the reinforcements are marked in Figure 3 by dots. As seen, there are two locations where the tensile stresses have peak values. The maximums on the left sides are always within the zone of the shear strain concentration just at the back of the blocks. It may be realized, the maximums on the right side are very close to the apparent failure line. Typical tensile force diagram is illustrated in Figure 6.

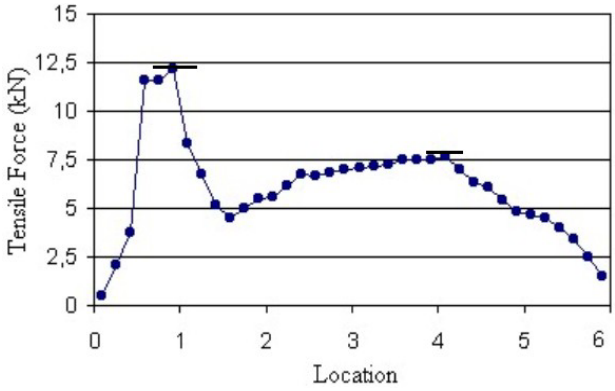

Figure 6. Tensile Forces on the sixth reinforcement in B3

The apparent failure line at the end of the staged construction will never give the actual failure mechanism because, at the end of the staged construction, failure does not occur. The actual mechanism should be studied in the failure case. As a result, phi-c reduction was chosen to help to study the failure case. The failure is believed to occur in the calculation step where ΣMsf becomes almost steady (Figure 7). Evaluating the incremental shear strains at this calculation step will give us a good idea about the failure mechanism despite their values have no physical meaning as stated by the program's manual.

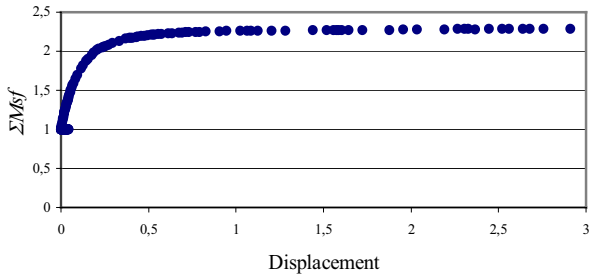

Figure 7. ΣMsf at the phi-c reduction

All the incremental shear strains between the staged construction and the phi-c reduction were successively put together by the

animation program to monitor the incremental shear strains trend. According to this animation, in model B3, the apparent failure line moves downwards changing into bilinear shape in the incremental shear strains output (Figure 8.). As *ΣMsf* is increased, the first piece of the apparent failure line inside the reinforced zone becomes flatter and comes closer to the bottom reinforcement levels. The second piece of the apparent failure line outside the reinforced zone moves downwards. Namely, the reinforced zone is drifted to the left and the unreinforced zone moves towards the reinforced zone like a wedge (Figure 9). The excessive plastic deformations occur within the lower 0-1.5 meters and the remaining upper reinforced body is drifted almost in an undeformed shape. Finally, if this mechanism and the shear strain development are considered together, the actual failure mechanism is found to be *bilinear* and *compound*. This can also be interpreted as the failure mechanism approaching to direct sliding mode.

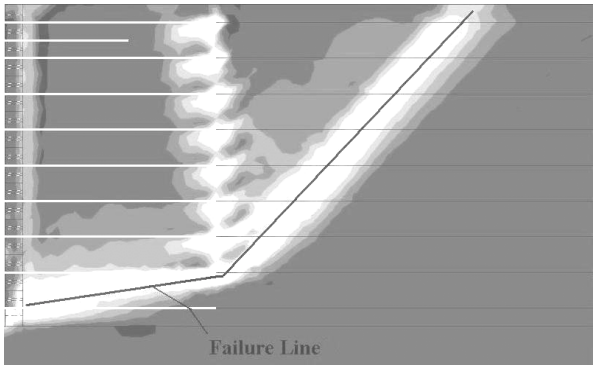

Figure 8. Incremental shear strain shadings at the end of phi-c reduction in B3

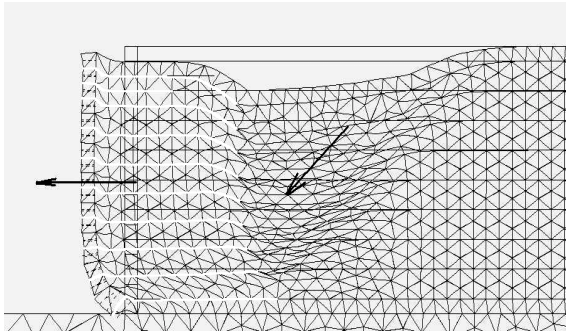

Figure 9. Deformed mesh at the end of phi-c reduction in B3 (displacements scaled up 2 times)

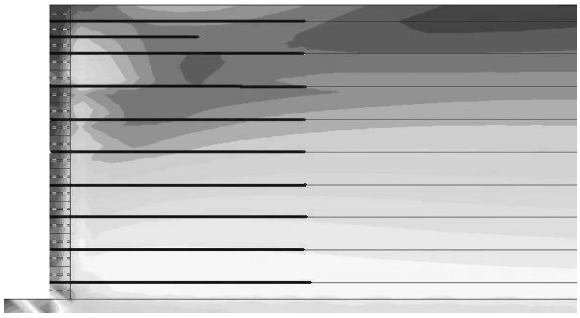

Figure 10. Shear strains shadings at the end of the staged construction in B4

B4 model is chosen to represent the cohesive backfill. The shear strains output at the end of the staged construction in B4 system is illustrated in Figure 10. Unlike in granular systems there is no certain shear strain zone forming at the end of the staged construction. The tensile forces on the reinforcements are very low compared to the tensile forces calculated in the granular backfill. They range between 1-3 kN/m. The maximum horizontal displacement of this cohesive system is 0.7 cm, which is smaller compared to the horizontal displacement in the granular B3 system. In phi-c reduction, where the *ΣMsf* value becomes stable, the incremental shear strains concentrate along a bilinear zone similar to the one obtained in granular systems (Figure 11). From these figures, we can say that failure mechanism of the systems with cohesive backfill is almost the same as the failure mechanism of the granular systems.

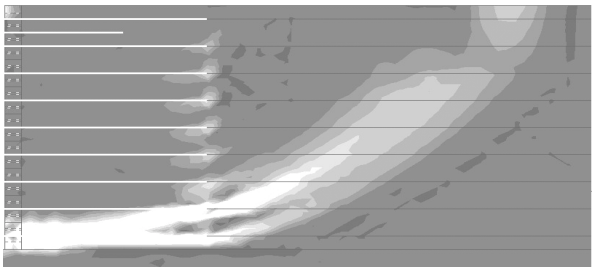

Figure 11. Incremental shear strain shadings at the end of phi-c reduction in B4

5 CONCLUSION

1. For granular backfills, the location of the shear strain concentration as obtained from Finite Element analysis coincides with the assumed failure plane of Limit Equilibrium analysis, but this is not the location where failure occurs.
2. For cohesive backfills, no internal failure mechanism develops at all under normal loading conditions.
3. In both type of soils the direct sliding mode seems to be the controlling mode at failure.
4. The tensile strength of the reinforcement is much less activated for cohesive backfill when compared to the granular backfill.
5. Both cohesive and granular soils seem to be adequate backfill materials.

6 REFERENCES

Brinkgreve, R.B.J. & Vermeer, P.A. 1998. Finite Element Code for Soil and Rock Analyses Version 7. Rotterdam: Balkema.

Elias, V. & Christopher, B.R. 1997. Mechanically stabilised earth walls and reinforced soil slopes, design and construction guidelines. In FHWA demonstration project 82 reinforced soil structures/August 1997. Springfield: National Technical Information Service.

Matsui, T. & San, K.C. 1988. Finite element stability analysis method for reinforced slope cutting. In International Geotechnical Symposium on Theory and Practice of Earth Reinforcement/Fukoka Japan/ 5-7 October 1988. Rotterdam: Balkema.

San, K. & Leshchinsky, D. & Matsui T. 1994. Geosynthetic reinforced slopes: Limit equilibrium and finite element analyses. In Soils and foundations Vol. 34 No. 2, 79-85 June 1994 Japanese Society of Soil Mechanics and Foundation Engineering

Smith, I.M. & Segrestin, P. 1992. Inextensible reinforcements versus extensible ties- FEM comparative analysis of reinforced or stabilized earth structures. In Earth Reinforcement Practice Ochaiai & Hayashi & Otani (eds). Rotterdam: Balkema.

Zornberg, J. G. & Sitar, N. & Mitchell J. K. 1998. Performance of geosynthetic reinforced slopes at failure. In Journal of geotechnical and geoenvironmental engineering/August 1988.